Available online at www.sciencedirect.com
SCIENCE DIRECT
Journal of Sound and Vibration 295 (2006) 214–225
JOURNAL OF SOUND AND VIBRATION
www.elsevier.com/locate/jsvi

Closed form solutions for the dynamic response of Euler–Bernoulli beams with step changes in cross section

Michael A. Koplow[a], Abhijit Bhattacharyya[a], Brian P. Mann[b,*]

[a]*Department of Mechanical and Aerospace Engineering, University of Florida, Gainesville, FL 32611, USA*
[b]*Department of Mechanical and Aerospace Engineering, University of Missouri-Columbia, Columbia, MO 65211, USA*

Received 25 August 2005; received in revised form 5 December 2005; accepted 3 January 2006
Available online 9 March 2006

Abstract

This paper provides an analytical solution for the dynamic response of a discontinuous beam with one step change and an aligned neutral axis. The case of free–free boundary conditions is considered to obtain direct frequency response functions due to harmonic force or couple excitation at either end location. This behavior is confirmed through a series of experimental tests and via comparison to receptance coupling methods.

1. Introduction

Beams provide a fundamental model for the structural elements of many engineering applications. For instance, helicopter rotor blades, spacecraft antennae, and robot arms are all examples of structures that may be modeled with beam-like elements [1,2]. The work presented in this paper grew out of the need to examine an industrial machining process where the dynamic response of a beam-like structure was the primary limiting factor—see Refs. [3–6] for explanations of machining stability. This material removal process additionally presented two unique challenges: (1) a change in the beam's dynamic response and machining stability limit as each layer of material was incrementally removed; and (2) a discontinuity in the beam structure which prevented direct application of conventional beam theory. While the literature for machining stability prediction is widely available, the goal of this paper is to present analytical solutions for the dynamic response of a discontinuous beam that were developed to better understand the aforementioned industrial process.

A literature survey has shown that the dynamic response for the transverse vibration of continuous Euler–Bernoulli beams has been well studied using both modal superposition techniques [7] and receptance techniques [8]. The static behavior of Euler–Bernoulli beams with jump discontinuities has been studied using generalized solutions [9–11]. The free vibration of stepped beams with aligned neutral axes has previously been treated to find natural frequencies and mode shapes expressed as determinants equated to zero [12–14]. While previous works have treated the free vibration case, the present paper investigates the dynamic response of stepped beams.

*Corresponding author. Tel.: +1 573 882 8160.
E-mail address: mannbr@missouri.edu (B.P. Mann).

0022-460X/$ - see front matter © 2006 Elsevier Ltd. All rights reserved.
doi:10.1016/j.jsv.2006.01.008

Alternative coupling techniques, such as receptance coupling substructure synthesis [15–17], can also be used to examine the dynamic behavior of discontinuous beams. Substructuring methods allow the prediction of assembly frequency response functions (FRFs) using FRFs from individual components obtained either analytically or experimentally. The solution forms a 2×2 matrix of the primary receptances of the individual beam components for each frequency. The technique requires an inversion of the 2×2 matrices per frequency. For high-resolution FRFs, the solution becomes computationally expensive.

In this paper, an analytical solution for the dynamic response of a free–free discontinuous beam with a single step change and an aligned neutral axis is considered. The phrase "aligned neutral axis" is applied to specifically distinguish the case where the neutral axis of both beams coincide; this is in contrast to the case where the neutral axis of the beams may be offset. Analytical results are verified by receptance coupling methods and experiment. One limitation of this work is that a partial differential equation is needed to obtain an assumed mode shape solution. Additionally, the described approach requires information about the compatibility conditions between individual components. The presented work can easily be extended to beams with n-beam sections and other classical boundary conditions. The solution process is reduced to solving a set of $4n$ equations with $4n$ variables.

2. Receptance derivation for discontinuous Euler–Bernoulli beams

This section develops the receptance functions for the case of free boundary conditions at the end locations with one step change in cross section as shown in Fig. 1. The discontinuity is treated by assuming two separate uniform Euler–Bernoulli beams coupled with continuity conditions at location B. The problem is solved as a boundary value problem with eight unknown constants.

2.1. Uniform beam receptances

This section examines the receptance function solutions for the uniform beam. The discontinuous beam will be shown to be an extension of the uniform beam. The governing equation for the free vibration of a uniform Euler–Bernoulli beam is given in Ref. [7] as

$$\frac{\partial^2 v(x,t)}{\partial t^2} + \frac{EI}{\rho A}\frac{\partial^4 v(x,t)}{\partial x^4} = 0, \tag{1}$$

where E is the beam modulus of elasticity (N/m^2), A is the beam cross-sectional area (m^2), ρ is the beam density (kg/m^3), I is the second area moment of inertia about the neutral axis (m^4), v is the transverse deflection, and t and x are time and space, respectively. The Euler–Bernoulli approximation assumes that the length of each beam section is much greater than the height of each section and that the shear and rotary inertia effects are ignored. The solution to Eq. (1), when subjected to a harmonic input of frequency ω (rad/s), can be separated into a solution in space and time

$$v = X(x)\sin\omega t. \tag{2}$$

Substitution of Eq. (2) into Eq. (1) yields dependence upon the spatial quantity alone,

$$\frac{\partial^4 X(x)}{\partial x^4} - \beta^4 X(x) = 0, \tag{3}$$

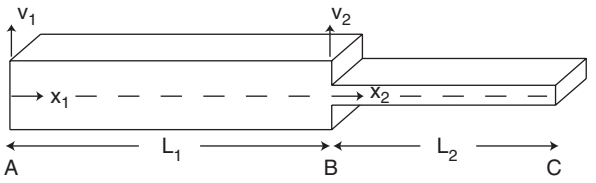

Fig. 1. Schematic of the stepped beam with aligned neutral axis and free boundary conditions at locations A and C.

where $\beta^4 = \omega^2\rho A/(EI(1+i\eta))$ and η is a non-dimensional structural damping factor. The general mode shape solution to $X(x)$ is

$$X(x) = A\sin\beta x + B\cos\beta x + C\sinh\beta x + D\cosh\beta x, \tag{4}$$

where A, B, C, and D are constants determined by suitable boundary conditions. The free vibration solution is 4×4 determinant obtained by applying four boundary conditions to Eq. (4). The forced vibration solution, given by Ref. [8], is obtained by equating applied forces into the boundary conditions. Applied harmonic forces are equated to the shear force while applied harmonic couples are equated to the bending moment. The signs on the forces are determined by the positive sign convention as shown in Fig. 2. The FRF is obtained by solving a set of four equations with four variables.

2.2. Discontinuous stepped beam solution for force excitation at location C

This section develops the frequency response for force excitation at position C as shown in Fig. 3. The solution for the first beam section (A–B) is given by

$$X_1(x_1) = c_1\sin\beta_1 x_1 + c_2\cos\beta_1 x_1 + c_3\sinh\beta_1 x_1 + c_4\cosh\beta_1 x_1, \tag{5}$$

where the subscript 1 refers to the (A–B) beam section. The (A–B) beam sectional properties are given by E_1, I_1, ρ_1, and A_1. β_1 is given by $\beta_1^4 = \omega^2\rho_1 A_1/(E_1 I_1(1+i\eta))$.

Applying the free boundary condition at location A requires

$$\frac{\partial^2 v_1(0)}{\partial x_1^2} = \frac{\partial^3 v_1(0)}{\partial x_1^3} = 0. \tag{6}$$

Substituting Eq. (6) into Eq. (5) yields $c_1 = c_3$ and $c_2 = c_4$. The resulting expression becomes

$$X_1(x_1) = c_1(\sin\beta_1 x_1 - \sinh\beta_1 x_1) + c_2(\cos\beta_1 x_1 - \cosh\beta_1 x_1). \tag{7}$$

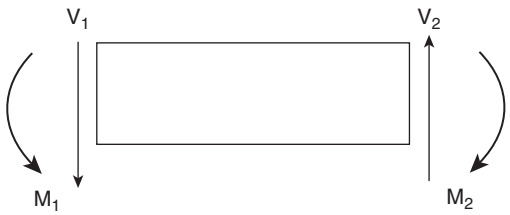

Fig. 2. Sign convention for positive bending moment (M) and shear force (V) for the Euler–Bernoulli beam.

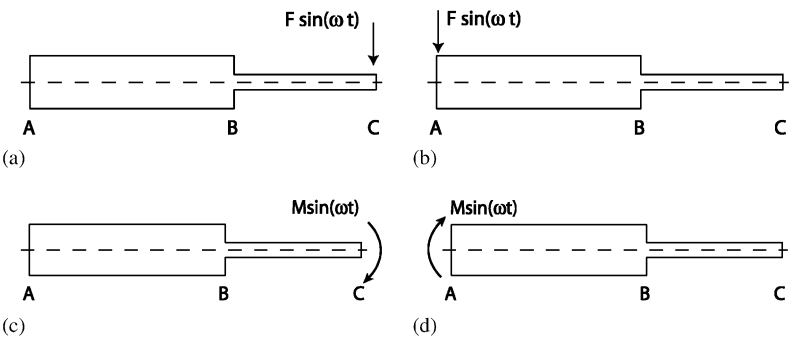

Fig. 3. Schematic of the stepped beam subjected to: (a) a harmonic force of amplitude F and frequency ω, applied at location C; (b) a harmonic force of amplitude F and frequency ω, applied at location A; (c) a harmonic couple of amplitude M and frequency ω, applied at location C; and (d) a harmonic couple of amplitude M and frequency ω, applied at location A.

The solution for the second beam section (B–C) is given by

$$X_2(x_2) = c_5 \sin \beta_2 x_2 + c_6 \cos \beta_2 x_2 + c_7 \sinh \beta_2 x_2 + c_8 \cosh \beta_2 x_2, \tag{8}$$

where the subscript 2 refers to the (B–C) beam section. The (B–C) beam sectional properties are given by E_2, I_2, ρ_2, and A_2, and β_2 is given by $\beta_2^4 = \omega^2 \rho_2 A_2/(E_2 I_2(1 + i\eta))$. It is understood that β_1 and β_2 are functions of frequency and the explicit notation has been left out.

The continuity conditions at location B for the given case of a colinear neutral axis state that the deflection, slope, bending moment, and shear force are equal for the opposite sides of the joint. The analytical expressions for the continuity conditions state:

$$v_1(L_1) = v_2(0), \tag{9a}$$

$$\frac{dv_1(L_1)}{dx} = \frac{dv_2(0)}{dx}, \tag{9b}$$

$$E_1 I_1 \frac{d^2 v_1(L_1)}{dx^2} = E_2 I_2 \frac{d^2 v_2(0)}{dx^2}, \tag{9c}$$

$$E_1 I_1 \frac{d^3 v_1(L_1)}{dx^3} = E_2 I_2 \frac{d^3 v_2(0)}{dx^3}. \tag{9d}$$

Applying the continuity equations yields

$$\begin{bmatrix} F_1 c_1 + F_3 c_2 \\ F_3 c_1 - F_2 c_2 \\ F_1 c_1 + F_4 c_2 \\ -F_4 c_1 + F_1 c_2 \end{bmatrix} = \begin{bmatrix} 0 & 1 & 0 & 1 \\ \beta_{21} I_{21} & 0 & \beta_{21} I_{21} & 0 \\ 0 & \beta_{21}^2 I_{21} & 0 & -\beta_{21}^2 I_{21} \\ -\beta_{21}^3 I_{21} & 0 & \beta_{21}^3 I_{21} & 0 \end{bmatrix} \begin{bmatrix} c_5 \\ c_6 \\ c_7 \\ c_8 \end{bmatrix}, \tag{10}$$

where

$$F_1 = \sin \beta_1 L_1 + \sinh \beta_1 L_1, \tag{11a}$$

$$F_2 = \sin \beta_1 L_1 - \sinh \beta_1 L_1, \tag{11b}$$

$$F_3 = \cos \beta_1 L_1 + \cosh \beta_1 L_1, \tag{11c}$$

$$F_4 = \cos \beta_1 L_1 - \cosh \beta_1 L_1, \tag{11d}$$

$$I_{21} = \frac{E_2 I_2}{E_1 I_1} \quad \text{and} \quad \beta_{21} = \frac{\beta_2}{\beta_1}. \tag{12}$$

The constants c_5, c_6, c_7, and c_8 can then be solved in terms of c_1 and c_2 using Eq. (10). The solution for $X_2(x)$ may now be expressed in terms of the remaining unknown constants c_1 and c_2:

$$\begin{aligned} X_2(x_2) = {} & c_1 \left(T_1 \sin \beta_2 x_2 + T_2 \cos \beta_2 x_2 + T_3 \sinh \beta_2 x_2 + T_4 \cosh \beta_2 x_2 \right) \\ & + c_2 \left(V_1 \sin \beta_2 x_2 + V_2 \cos \beta_2 x_2 + V_3 \sinh \beta_2 x_2 + V_4 \cosh \beta_2 x_2 \right), \end{aligned} \tag{13}$$

where

$$T_1 = \frac{F_4}{2 I_{21} \beta_{21}^3} + \frac{F_3}{2 \beta_{21}}, \tag{14a}$$

$$T_2 = \frac{F_2}{2 I_{21} \beta_{21}^2} + \frac{F_1}{2}, \tag{14b}$$

$$T_3 = -\frac{F_4}{2 I_{21} \beta_{21}^3} + \frac{F_3}{2 \beta_{21}}, \tag{14c}$$

$$T_4 = -\frac{F_2}{2I_{21}\beta_{21}^2} + \frac{F_1}{2}, \tag{14d}$$

$$V_1 = -\frac{F_1}{2I_{21}\beta_{21}^3} - \frac{F_2}{2\beta_{21}}, \tag{15a}$$

$$V_2 = \frac{F_4}{2I_{21}\beta_{21}^2} + \frac{F_3}{2}, \tag{15b}$$

$$V_3 = \frac{F_1}{2I_{21}\beta_{21}^3} - \frac{F_2}{2\beta_{21}}, \tag{15c}$$

$$V_4 = -\frac{F_4}{2I_{21}\beta_{21}^2} + \frac{F_3}{2}. \tag{15d}$$

Constants c_1 and c_2 are determined by the boundary conditions at location C. The boundary conditions at C require

$$\frac{\partial^2 v_2(L_2)}{\partial x_2^2} = 0, \tag{16a}$$

$$E_2 I_2 \frac{\partial^3 v_2(L_2)}{\partial x_2^3} = -F \sin \omega t. \tag{16b}$$

The boundary conditions state that the bending moment is equal to zero while the shear force is equal to the applied impulse load. Applying the conditions of Eq. (16) to Eq. (13) yields

$$c_1 Z_1 + c_2 Z_2 = 0, \tag{17a}$$

$$c_1 Z_3 + c_2 Z_4 = -\frac{F}{E_2 I_2}, \tag{17b}$$

where

$$\begin{bmatrix} Z_1 \\ Z_2 \\ Z_3 \\ Z_4 \end{bmatrix} = \begin{bmatrix} -T_1\beta_2^2 & -T_2\beta_2^2 & T_3\beta_2^2 & T_4\beta_2^2 \\ -V_1\beta_2^2 & -V_2\beta_2^2 & V_3\beta_2^2 & V_4\beta_2^2 \\ -T_1\beta_2^3 & T_2\beta_2^3 & T_3\beta_2^3 & T_4\beta_2^3 \\ -V_1\beta_2^3 & V_2\beta_2^3 & V_3\beta_2^3 & V_4\beta_2^3 \end{bmatrix} \begin{bmatrix} \sin \beta_2 L_2 \\ \sinh \beta_2 L_2 \\ \cos \beta_2 L_2 \\ \cosh \beta_2 L_2 \end{bmatrix}. \tag{18}$$

Solving Eq. (17) yields the frequency response solution

$$\frac{v}{F} = \frac{1}{(1+\mathrm{i}\eta)E_2 I_2 (Z_1 Z_4 - Z_2 Z_3)} [Z_2(T_1 \sin \beta_2 x_2 + T_2 \cos \beta_2 x_2 + T_3 \sinh \beta_2 x_2 + T_4 \cosh \beta_2 x_2) - Z_1(V_1 \sin \beta_2 x_2 + V_2 \cos \beta_2 x_2 + V_3 \sinh \beta_2 x_2 + V_4 \cosh \beta_2 x_2)], \tag{19}$$

where the compound beam is forced at position C, x_2 represents the spatial output location, and η represents the structural damping factor. The denominator $Z_1 Z_4 - Z_2 Z_3 = 0$ forms the so called frequency equation whose roots are the natural frequencies of the system.

2.3. Discontinuous stepped beam solution for force excitation at location A

This section develops the frequency response for force excitation at position A as shown in Fig. 3(b). The continuity conditions are the same as discussed above, however the boundary conditions at location A require

$$\frac{\partial^2 v_1(0)}{\partial x_2^2} = 0, \tag{20a}$$

Table 1
Notation for force excitation at position A

$$Z_5 = -T_2\beta_1^2 + T_4\beta_1^2$$
$$Z_6 = -V_2\beta_1^2 + V_4\beta_1^2$$
$$Z_7 = -T_1\beta_1^3 + T_3\beta_1^3$$
$$Z_8 = -V_1\beta_1^3 + V_3\beta_1^3$$

$$F_5 = \sin\beta_2 L_2 \sinh\beta_2 L_2 + \cosh\beta_2 L_2 \cos\beta_2 L_2$$
$$F_6 = -\sin\beta_2 L_2 \cosh\beta_2 L_2 + \sinh\beta_2 L_2 \cos\beta_2 L_2$$
$$F_7 = \sinh\beta_2 L_2 \cos\beta_2 L_2 + \sin\beta_2 L_2 \cosh\beta_2 L_2$$
$$F_8 = -\sin\beta_2 L_2 \sinh\beta_2 L_2 + \cosh\beta_2 L_2 \cos\beta_2 L_2$$

$$T_5 = \sin\beta_1 L_1\left(\tfrac{I_{21}\beta_{21}^2}{2}F_6 + \tfrac{F_6}{2}\right) + \cos\beta_1 L_1\left(\tfrac{I_{21}\beta_{21}^3}{2}(F_5 - 1) + \tfrac{\beta_{21}}{2}(F_5 + 1)\right)$$
$$T_6 = \sin\beta_1 L_1\left(\tfrac{I_{21}\beta_{21}^3}{2}(1 - F_5) - \tfrac{\beta_{21}}{2}(F_5 + 1)\right) + \cos\beta_1 L_1\left(\tfrac{I_{21}\beta_{21}^2}{2}F_6 + \tfrac{F_6}{2}\right)$$
$$T_7 = \sinh\beta_1 L_1\left(\tfrac{I_{21}\beta_{21}^2}{2}F_6 - \tfrac{F_6}{2}\right) + \cosh\beta_1 L_1\left(\tfrac{I_{21}\beta_{21}^3}{2}(1 - F_5) + \tfrac{\beta_{21}}{2}(F_5 + 1)\right)$$
$$T_8 = \sinh\beta_1 L_1\left(\tfrac{I_{21}\beta_{21}^3}{2}(F_5 - 1) - \tfrac{\beta_{21}}{2}(F_5 + 1)\right) + \cosh\beta_1 L_1\left(\tfrac{F_6}{2} - \tfrac{I_{21}\beta_{21}^2}{2}F_6\right)$$

$$V_5 = \sin\beta_1 L_1\left(\tfrac{I_{21}\beta_{21}^2}{2}(F_8 - 1) + \tfrac{1}{2}(F_8 + 1)\right) + \cos\beta_1 L_1\left(\tfrac{I_{21}\beta_{21}^3}{2}F_7 + \tfrac{\beta_{21}}{2}F_7\right)$$
$$V_6 = -\sin\beta_1 L_1\left(\tfrac{I_{21}\beta_{21}^3}{2}F_7 + \tfrac{\beta_{21}}{2}F_7\right) + \cos\beta_1 L_1\left(\tfrac{I_{21}\beta_{21}^2}{2}(F_8 - 1) + \tfrac{1}{2}(F_8 + 1)\right)$$
$$V_7 = \sinh\beta_1 L_1\left(\tfrac{I_{21}\beta_{21}^2}{2}(F_8 - 1) - \tfrac{1}{2}(F_8 + 1)\right) + \cosh\beta_1 L_1\left(\tfrac{\beta_{21}}{2}F_7 - \tfrac{I_{21}\beta_{21}^3}{2}F_7\right)$$
$$V_8 = \sinh\beta_1 L_1\left(\tfrac{I_{21}\beta_{21}^3}{2}F_7 - \tfrac{\beta_{21}}{2}F_7\right) + \cosh\beta_1 L_1\left(\tfrac{I_{21}\beta_{21}^2}{2}(1 - F_8) + \tfrac{1}{2}(F_8 + 1)\right)$$

$$E_2 I_2 \frac{\partial^3 v_1(0)}{\partial x_2^3} = F\sin\omega t. \tag{20b}$$

The sign change on the forcing term is due to the free body sign convention as shown in Fig. 2. The boundary conditions at location C now require

$$\frac{\partial^2 v_2(L_2)}{\partial x_2^2} = \frac{\partial^3 v_2(L_2)}{\partial x_2^3} = 0. \tag{21}$$

Using the same procedure as outlined before, the response of the compound beam to harmonic excitation is obtained. However, for loading at position A, the order of the procedure is reversed. In this case, the boundary conditions at location C are applied first, then the continuity conditions at location B, and then finally the boundary conditions at location A. Using the method as outlined before, the solution becomes

$$\frac{v}{F} = \frac{1}{(1+\mathrm{i}\eta)E_1 I_1(Z_5 Z_8 - Z_6 Z_7)}[Z_5(V_5\sin\beta_1 x_1 + V_6\cos\beta_1 x_1 + V_7\sinh\beta_1 x_1 + V_8\cosh\beta_1 x_1) - Z_6(T_5\sin\beta_1 x_1 + T_6\cos\beta_1 x_1 + T_7\sinh\beta_1 x_1 + T_8\cosh\beta_1 x_1)], \tag{22}$$

where the compound beam is loaded at position A. Additional terms are applied to reduce notation. The constants are defined in Table 1, where β_{21} and I_{21} are the same as above.

3. Extension of the analytical solution for applied couples and other boundary conditions

This section examines the case of applied harmonic couples as shown in Figs. 3(c) and (d). For both systems, the continuity conditions are the same as discussed above. For excitation at location C, the boundary

conditions at position A require

$$\frac{\partial^2 v_1(0)}{\partial x_1^2} = \frac{\partial^3 v_1(0)}{\partial x_1^3} = 0. \tag{23}$$

Due to the free body sign convention, the boundary conditions at position C now require

$$E_2 I_2 \frac{\partial^2 v_1(L_2)}{\partial x_2^2} = M \sin \omega t, \tag{24a}$$

$$\frac{\partial^3 v_2(L_2)}{\partial x_2^3} = 0. \tag{24b}$$

For excitation at position A, the boundary conditions at location C require

$$\frac{\partial^2 v_2(L_2)}{\partial x_2^2} = \frac{\partial^3 v_2(L_2)}{\partial x_2^3} = 0, \tag{25}$$

while the boundary conditions at location A require

$$E_1 I_1 \frac{\partial^2 v_1(0)}{\partial x_1^2} = -M \sin \omega t, \tag{26a}$$

$$\frac{\partial^3 v_1(0)}{\partial x_1^3} = 0. \tag{26b}$$

The system FRFs are obtained using the same procedure as outlined before. Boundary conditions at the unforced end are applied first, then the continuity conditions, and then the boundary conditions at the point of excitation.

Applications due to other classical boundary conditions are straightforward. In exchange for the free condition of zero shear and zero bending moment at the unforced end, the boundary conditions become $v = \partial v/\partial x = 0$ for a fixed end, $v = \partial^2 v/\partial x^2 = 0$ for a pinned end, and $\partial v/\partial x = \partial^3 v/\partial x^3 = 0$ for a sliding end.

3.1. Comparison of the analytical solution to receptance coupling

This section compares the responses given by the proposed analytical solution and receptance coupling substructure synthesis. Receptance coupling is an alternative method capable of predicting the dynamic response of the stepped beam. The receptance coupling method involves coupling the receptances for uniform beams obtained analytically or experimentally at the discontinuity using compatibility conditions. The end result is a 2×2 matrix for each frequency consisting of the primary receptances given by the individual beam components. The component matrices are written as

$$R_{11} = \begin{bmatrix} h_1 & l_1 \\ n_1 & p_1 \end{bmatrix} = \begin{bmatrix} \dfrac{x_1}{f_1} & \dfrac{x_1}{m_1} \\ \dfrac{\theta_1}{f_1} & \dfrac{\theta_1}{m_1} \end{bmatrix}, \tag{27}$$

where the subscripts indicate either direct or cross receptances due to applied component forces and moments at the coordinates shown in Fig. 4. The individual beam receptances, h, l, n, and p, are frequency-dependent vectors such that the size of the total matrix is $2 \times 2 \times N$ where N is the length of the frequency vector. The entries into the matrices are found from a model of the free–free beams based upon Ref. [8]. The solution for the case of excitation at location C, given by receptance coupling [15], is

$$G_{11} = R_{11} - R_{12}(R_{22} + R_{2b2b})^{-1} R_{21}, \tag{28}$$

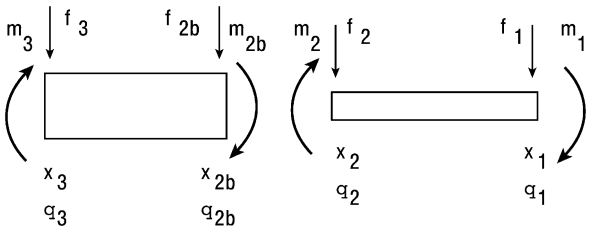

Fig. 4. Schematic diagram of the separated components used for the receptance coupling analysis approach.

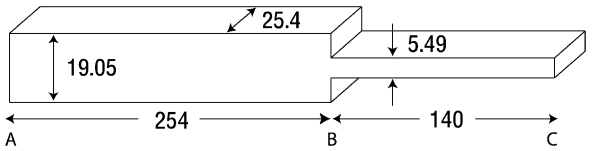

Fig. 5. Dimensions for the beam used for experimental and analytical study. All length dimensions are given in units of mm.

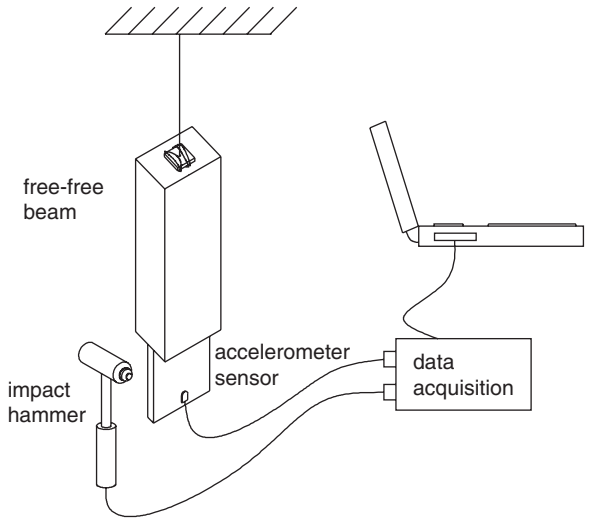

Fig. 6. Schematic of the experimental tests performed to validate the analytical studies. The discontinuous beam was suspended from a nylon thread that was attached the end of the beam.

where the desired deflection FRF due to an applied force is the first entry in the matrix for each frequency. The solution for the case of excitation at location A is

$$G_{33} = R_{33} - R_{32b}(R_{22} + R_{2b2b})^{-1} R_{2b3}. \tag{29}$$

To compare the proposed solution and the receptance coupling result, consider the model given in Fig. 5. The model consists of a stepped beam with a rectangular cross section and colinear neutral axis. The material is 7050 aluminum with a density of $\rho = 2830\,\mathrm{kg/m^3}$, a Young's modulus of $E = 71.7\mathrm{e}9\,\mathrm{Pa}$, and structural damping factor of $\eta = 0.02$. Both beam sections consist of the same material with the same damping factor (Fig. 6).

Figs. 7 and 8 show a comparison of the real and imaginary portions of the FRFs obtained via Sections 2.2 and 2.3 to the receptance coupling solution. The results show that the solutions are identical. However, the advantage of the proposed solution method is in the processing power required to obtain the solutions. As shown in Eqs. (28) and (29), the receptance coupling solution requires inverting the matrices for each frequency of interest. As the frequency vector becomes large, either due to more frequency resolution or larger

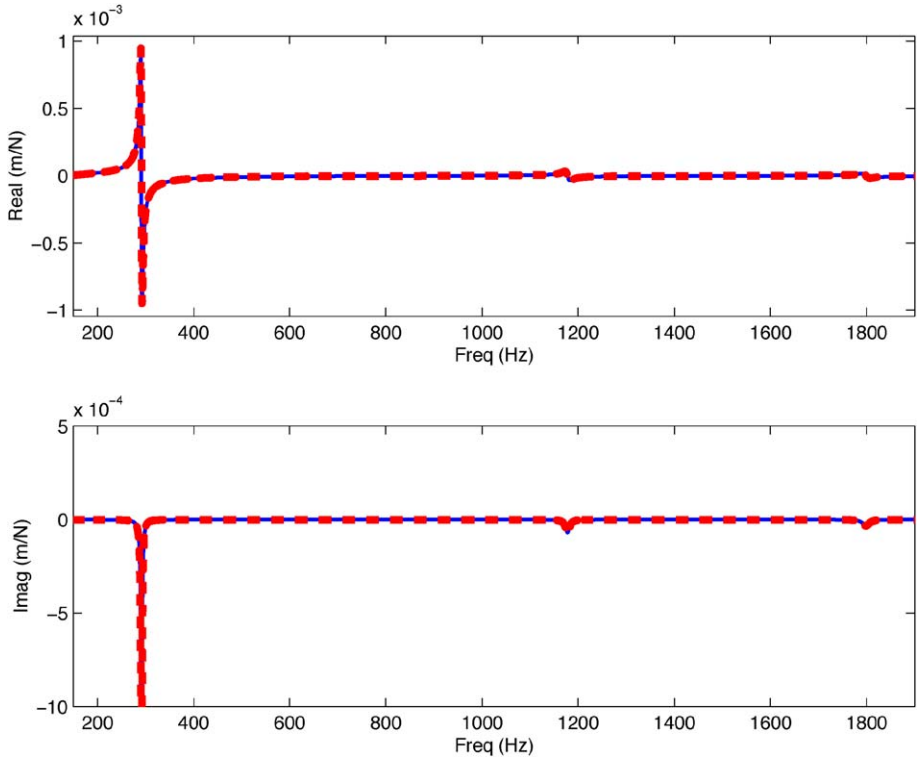

Fig. 7. FRF comparison between analytical (solid) and receptance coupling (dashed) methods when forced at position C.

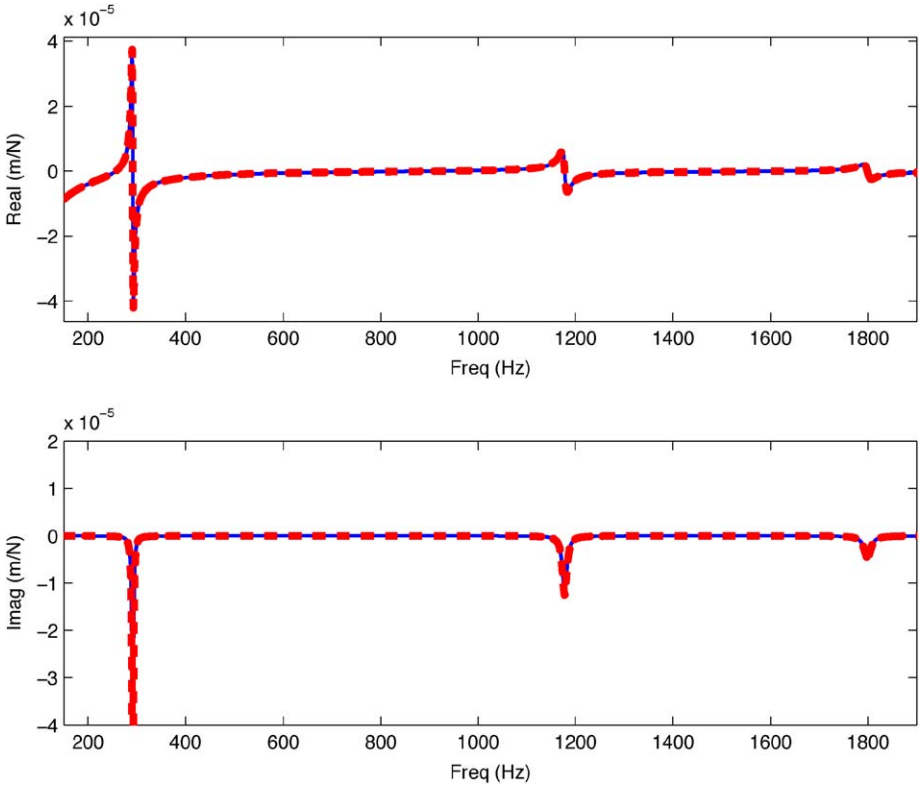

Fig. 8. FRF comparison between analytical (solid) and receptance coupling (dashed) methods when forced at position A.

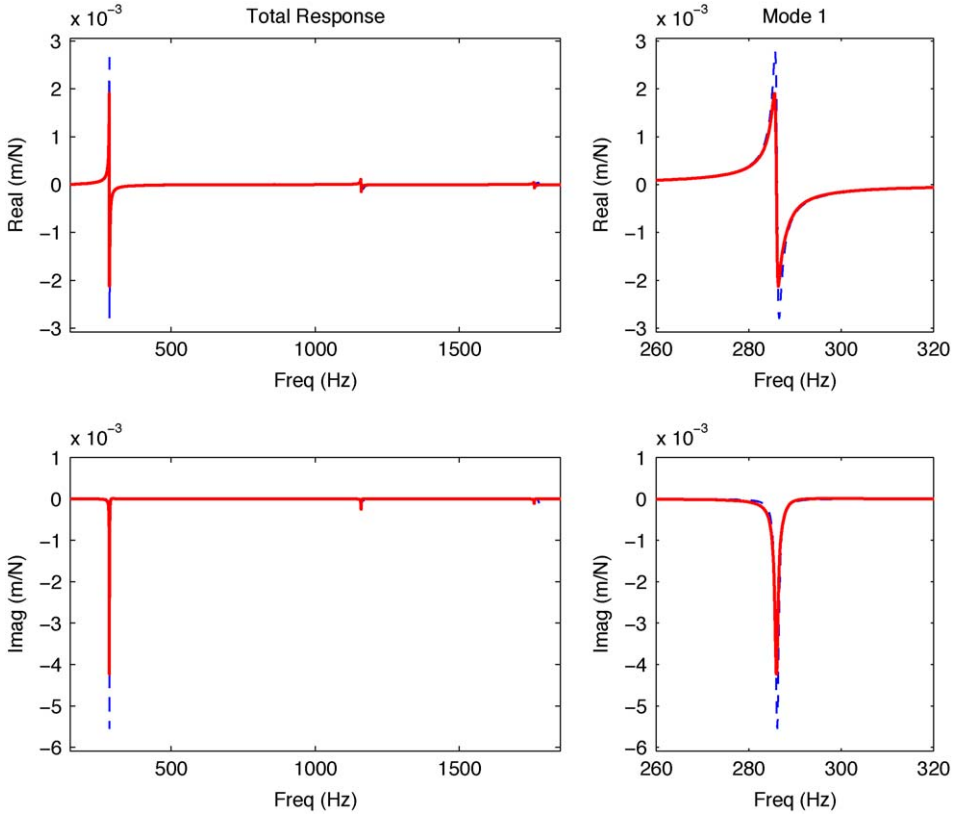

Fig. 9. Comparison of experimental (solid) and analytical (dashed) FRF when forced at position C.

frequency bandwidth, the function becomes very costly to perform. The proposed solution, however, requires far less computing power for large frequency vectors.

4. Experimental verification

This section provides experimental verification for the analyses of Sections 2.2 and 2.3. The experiment consists of a stepped beam of 7050 aluminum with dimensions given in Fig. 4. The material has a density of $\rho = 2830\,\mathrm{kg/m^3}$ and a Young's modulus of $E = 71.7\mathrm{e}9\,\mathrm{Pa}$. Structural damping was obtained as a best fit approximation to the data. For excitation at location C, a damping value $\eta = 0.003$ was obtained. For excitation at location A, the damping value was determined to be $\eta = 0.001$. The free–free boundary conditions were obtained by suspending the beam with a taut nylon string, rigidly attached to the end of the beam via a thin piece of plexi-glass as shown in Fig. 6. Experiments were conducted by impacting the beam with a PCB[1] modal hammer and obtaining the response with a PCB low mass accelerometer mounted onto the beam. For each of the reported FRFs, 10 or more individual impact test were recorded, and averaged in the frequency domain, to obtain the reported results.

To eliminate mass loading effects due to the inertia of the accelerometer, the analytical predictions were compensated to include the additional dynamics of the system. The correction for a driving point FRF is given by [18]

$$A_n = \frac{A}{1 - mA}, \tag{30}$$

[1]Commercial equipment is identified for completeness and does not necessarily imply endorsement by the authors.

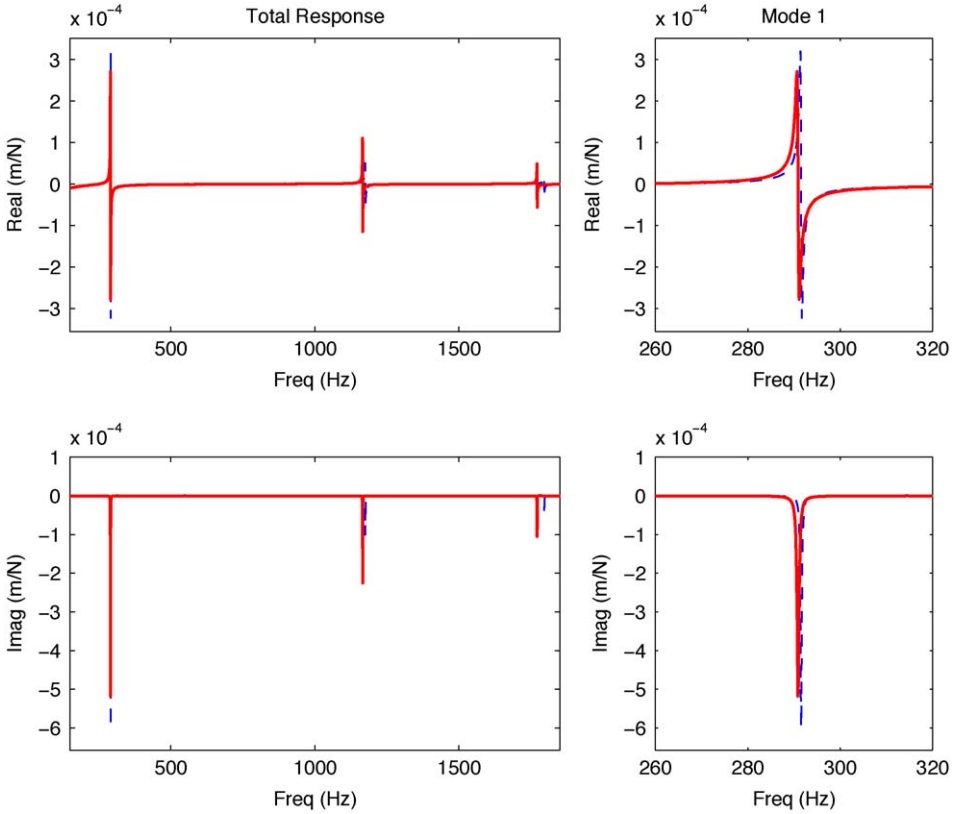

Fig. 10. Comparison of experimental (solid) and analytical (dashed) FRF when forced at position A.

where A_n represents the accelerance FRF of total system including the accelerometer mass, A represents the accelerance FRF of the original analytical system, and m is the extra mass of the accelerometer in the units of kg. The accelerance FRFs are obtained from the receptance FRFs by the relationship

$$\frac{v}{F} = \frac{A}{-\omega^2}, \tag{31}$$

where ω is the frequency vector in rad/s. As shown in Eq. (30), the mass loading effect is frequency dependent. Figs. 9 and 10 show the results for the experiments for the first three modes for direct FRFs at locations C and A, respectively. The accelerometer mass was measured to be $m = 0.7$ g.

The data shows experimental modes at 286, 1159, and 1759 Hz for the experimental test measured at location C. Experimental modes for the test at location A were found to be located at 291, 1165, and 1771 Hz. The differences are due to additional relative inertia of the accelerometer when placed on the thinner cross section. As the data shows, the experimental results are in excellent agreement with the analytical predictions. Results show that analytical predictions are higher than the experimental measurements.

5. Summary and conclusions

Various researchers have previously calculated the natural frequencies of a discontinuous beam using analytical and approximate methods. The goal of this paper was to predict the dynamic response of discontinuous beams with one step change and an aligned neutral axis. The case of free–free boundary conditions has been treated to obtain the direct FRF due to harmonic force or couple excitation at either end location. The solution was represented as a boundary value problem whereby the constants are dependent on

the boundary conditions. A comparison to receptance coupling methods have been shown to be identical. The potential benefit of the proposed solution is less computational time for structures requiring high frequency bandwidth or resolution. Experimental impact testing was performed using low mass accelerometers and modal hammers to obtain the direct FRFs for the beam striking at either end location. The analytical predictions were corrected for the additional inertia caused by the accelerometer attachment. The impact tests have shown that the analytical predictions match experimental data with minimal errors.

Acknowledgements

Support from US National Science Foundation CAREER Award (CMS-0348288) is gratefully acknowledged.

References

[1] P. Sooraksa, G. Chen, Mathematical modeling and fuzzy control of a flexible-link robot arm, *Mathematical and Computer Modelling* 27 (6) (1998) 73–93.
[2] G. Surace, V. Anghel, C. Mares, Coupled bending-bending-torsion vibration analysis of rotating pretwisted blades: an integral formulation and numerical examples, *Journal of Sound and Vibration* 206 (1997) 473–486.
[3] J. Tlusty, *Manufacturing Processes and Equipment*, Prentice-Hall, Upper Saddle River, NJ, 2000.
[4] B.P. Mann, P.V. Bayly, M.A. Davies, J.E. Halley, Limit cycles, bifurcations, and accuracy of the milling process, *Journal of Sound and Vibration* 277 (2004) 31–48.
[5] T. Insperger, G. Stépán, P.V. Bayly, B.P. Mann, Multiple chatter frequencies in milling processes, *Journal of Sound and Vibration* 262 (2003) 333–345.
[6] B.P. Mann, K.A. Young, T.L. Schmitz, D.N. Dilley, Simultaneous stability and surface location error predictions in milling, *Journal of Manufacturing Science and Engineering* 127 (2005) 446–453.
[7] L. Meirovitch, *Elements of Vibration Analysis*, second ed., McGraw-Hill, Inc., New York, 1986.
[8] R. Bishop, D. Johnson, *The Mechanics of Vibration*, Cambridge University Press, Cambridge, 1960.
[9] A. Yavari, S. Sarkani, J.N. Reddy, Generalized solutions of beams with jump discontinuities on elastic foundations, *Archive of Applied Mechanics* 71 (2001) 625–639.
[10] A. Yavari, S. Sarkani, E.T. Moyer, On applications of generalized functions to beam bending problems, *International Journal of Solids and Structures* 37 (2000) 5675–5705.
[11] B. Biondi, S. Caddemi, Closed form solutions of Euler–Bernoulli beams with singularities, *International Journal of Solids and Structures* 42 (2005) 3027–3044.
[12] S. Naguleswaran, Natural frequencies, sensitivity, and mode shape details of an Euler–Bernoulli beam with one-step change in cross-section with ends on classical supports, *Journal of Sound and Vibration* 252 (2002) 751–767.
[13] M.A. DeRosa, Free vibrations of stepped beams with elastic ends, *Journal of Sound and Vibration* 173 (4) (1994) 563–567.
[14] T. Tsukazan, The use of a dynamical basis for computing the modes of a beam system with a discontinuous cross-section, *Journal of Sound and Vibration* 281 (2005) 1175–1185.
[15] T. Schmitz, R. Donaldson, Predicting high-speed machining dynamics by substructure analysis, *Annals of the CIRP* 49 (1) (2000) 303–308.
[16] T.L. Schmitz, G.S. Duncan, Receptance coupling for dynamics prediction of assemblies with coincident neutral axes, *Journal of Sound and Vibration* 289 (2006) 1045–1065.
[17] S.S. Park, Y. Altintas, M. Movahhedy, Receptance coupling for end mills, *International Journal of Machine Tools and Manufacture* 43 (2003) 889–896.
[18] M.R. Ashory, High Quality Modal Testing Methods, PhD Thesis, Imperial College of Science, Technology and Medicine, London, 1999.